Characteristic length scale of the magnon accumulation in Fe$_3$O$_4$/Pt bilayer structures by incoherent thermal excitation

A. Anadón,[1,2,a)] R. Ramos,[3,4] I. Lucas,[1,2] P. A. Algarabel,[2,5] L. Morellón,[1,2] M. R. Ibarra,[1,2,6] and M. H. Aguirre[1,2,6]

[1]*Instituto de Nanociencia de Aragón, Universidad de Zaragoza, E-50018 Zaragoza, Spain*
[2]*Departamento de Física de la Materia Condensada, Universidad de Zaragoza, E-50009 Zaragoza, Spain*
[3]*WPI Advanced Institute for Materials Research, Tohoku University, Sendai 980-8577, Japan*
[4]*Spin Quantum Rectification Project, ERATO, Japan Science and Technology Agency, Sendai 980-8577, Japan*
[5]*Instituto de Ciencia de Materiales de Aragón, Universidad de Zaragoza and Consejo Superior de Investigaciones Científicas, 50009 Zaragoza, Spain*
[6]*Laboratorio de Microscopías avanzadas, Universidad de Zaragoza, 50018 Zaragoza, Spain*

The dependence of Spin Seebeck effect (SSE) with the thickness of the magnetic materials is studied by means of incoherent thermal excitation. The SSE voltage signal in Fe$_3$O$_4$/Pt bilayer structure increases with the magnetic material thickness up to 100 nm, approximately, showing signs of saturation for larger thickness. This dependence is well described in terms of a spin current pumped in the platinum film by the magnon accumulation in the magnetic material. The spin current is generated by a gradient of temperature in the system and detected by the Pt top contact by means of inverse spin Hall effect. Calculations in the frame of the linear response theory adjust with a high degree of accuracy the experimental data, giving a thermal length scale of the magnon accumulation (Λ) of 17 ± 3 nm at 300 K and $\Lambda = 40 \pm 10$ nm at 70 K. *Published by AIP Publishing.* [http://dx.doi.org/10.1063/1.4955031]

The generation of spin currents by a thermal gradient has been a very active field of study since the discovery of the Spin Seebeck effect (SSE) in a permalloy film.[1] The SSE consists in the generation of a spin voltage as a result of a temperature gradient in a magnetic material (FM). Two different geometrical configurations have been used to measure the SSE: the transversal and longitudinal (LSSE) configurations. In the transversal configuration the thermal gradient and magnetic field are parallel and the voltage generated is measured perpendicular to both the magnetic field and the interface normal.[1] This configuration has been utilized widely due to the experimental simplicity, but is applicable only to a few systems, since the mismatch of thermal conductivity between substrate and film can induce parasitic effects that contaminate the signal, such as the anomalous Nernst effects (ANEs) and planar Nernst effects (PNEs) in conductive ferromagnets.[2,3] In LSSE[4] the thermal gradient applied is perpendicular to the applied magnetic field and the voltage generated is measured in a direction perpendicular to both of them as shown in Figure 1(I-a). It has been recently suggested that the SSE generates from bulk magnonic spin currents in magnetic insulators,[5,6] not only the spin current generated at the interface with a non magnetic layer (NM).[7] The spin current is detected in the NM by the inverse spin hall effect (ISHE).[8]

Two length scales are involved in magnon transport: one related with inelastic scattering and accessible by thermal conductivity measurements;[9,10] the other one is associated with spin-flip scattering and relevant in experiments of SSE when varying the film thickness.[6,11–13]

The magnitude of the spin current injected in NM is determined by the magnon spin current in FM and the boundary conditions. The output voltage in the NM layer depends on both NM and FM layer thickness[5] opening the possibility to better understand the physical properties involved to optimize the SSE signal in order to increase the output power. Other experimental parameters have to be considered to enhance the signal such as crystal quality of the FM and NM, the number of multilayers,[14] thermal conductivity mismatch between substrate and films, and the FM/NM interface quality.

It has been predicted[15] and reported recently[6] that thermally excited magnons created in the bulk material have a finite propagation length which could lead to the saturation of the SSE signal. This behavior can be explained using the linear response theory of the SSE[16] as well as Boltzmann equation.[17,18] In this work the model reported by Adachi *et al.*[16] is used to fit our experimental data, which considers the spin diffusion in the ferromagnet and obtains the thermal length scale of the magnon accumulation (Λ) from the magnon diffusion equation. Another parameter to take into account is the damping constant of the ferromagnet since it affects the distribution of magnon temperatures.[6]

In this paper we study the SSE on Fe$_3$O$_4$/Pt bilayers as a function of the FM thickness. The Fe$_3$O$_4$ epitaxial thin films with thickness from 10 to 280 nm were deposited on a (001) magnesium oxide (MgO) substrate by means of pulsed laser deposition (PLD). Pt was sputtered following different procedures and thickness: (1) 14 nm *in-situ* growth at 400 °C, (2) 17, 13.5, 8.5 nm *ex-situ* growth at 200 °C, and (3) 14 nm *ex-situ* growth at room temperature. Further details on the growth conditions can be found elsewhere.[19] Sample magnetization and resistivity of the samples and its dependence

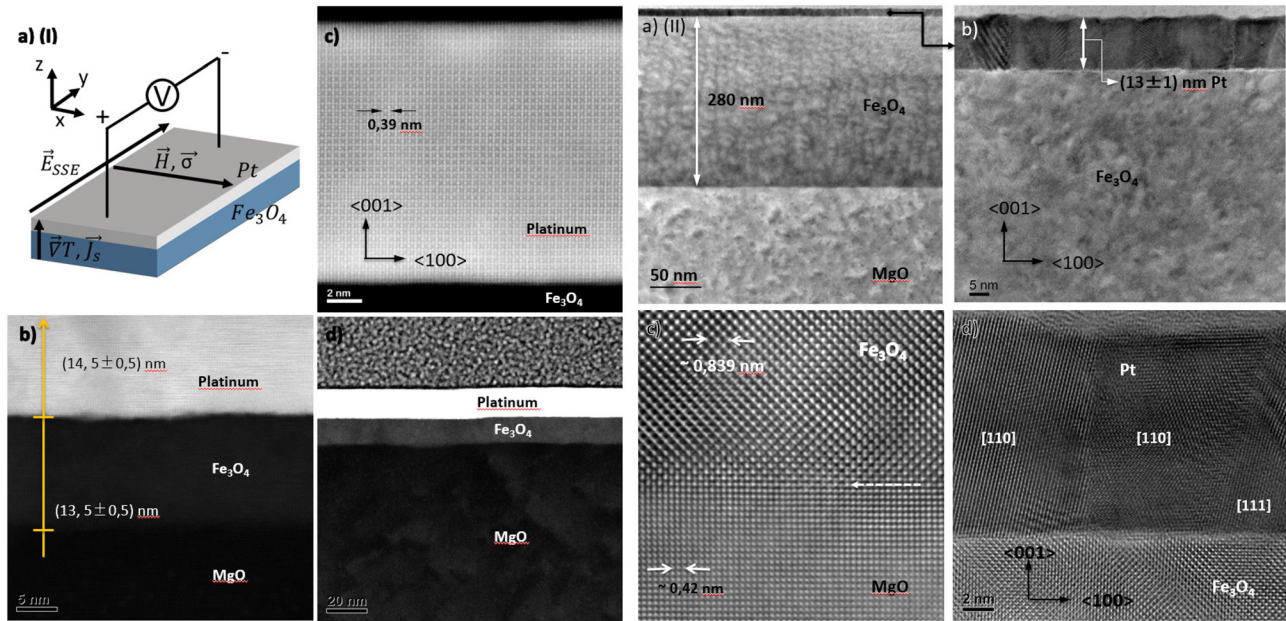---

a)Electronic mail: anadonb@unizar.es

FIG. 1. (I) STEM-HAADF images by probe corrected FEI Titan 60-300 and LSSE geometry. (a) LSSE geometry scheme; (b) Image of Pt/Fe$_3$O$_4$/MgO with thickness description and showing epitaxial growth; (c) Detail of epitaxial Pt top layer; (d) General view of bilayer system and MgO substrate; (II) Bright field images by aberration corrected FEI Titan Cube. (a) General view of thick film Pt/Fe$_3$O$_4$/MgO, Pt in dark, Fe$_3$O$_4$ dark gray and MgO light gray contrast, respectively; (b) HRTEM image of Pt grains of the contact showing columnar growth typical for Pt deposition in vacuum chamber at high temperature and clean conditions; (c) HRTEM of sharp interface Fe$_3$O$_4$/MgO and showing epitaxial growth (see the arrow); (d) HRTEM image of Pt contact, detail of grain orientations, in [110] zone axis and one along [111] zone axis; note the sharp interface with Fe$_3$O$_4$ for both Pt grains on magnetite film.

with temperature and thickness were also found to be consistent with previous studies.[20,21]

The crystalline structure was analyzed using X-ray diffraction (XRD), high-resolution TEM and scanning transmission electron microscopy with high-angle annular dark-field detector (STEM-HAADF). In XRD, Laue oscillations are observed in all the samples below 100 nm indicating high crystalline coherence. This was confirmed by STEM-HAADF images [Figure 1(I-d)] that also show very small interdiffusion of about one unit cell of Fe$_3$O$_4$ in the MgO substrate. Antiphase boundaries (APBs) are also observed in TEM studies [see Figures 1(I-d), 1(II-b), and 1(II-d)] as expected for an MgO/Fe$_3$O$_4$ system. The different processes of Pt deposition yielded different nanostructure of the platinum contact. For samples grown every step *in situ* in preparation chamber at high vaccum, Pt is fully epitaxial with MgO/Fe$_3$O$_4$ [see Figures 1(I-b), 1(I-c), and 1(I-d)], while for *ex-situ* deposition, Pt was polycrystalline [see Figures 1(II-b) and (II-d)]. Another difference can be established depending on the deposition temperature. Pt deposited *ex-situ* at high temperature showed high crystalline grains in columnar growth with a size around 10 nm, with a few grain orientations in lower Miller index [see Figure 1(II-d)] and good interface with magnetite film, while Pt deposited at room temperature showed bad quality interface with magnetite and nanograins with size smaller than 4 nm. The difference in the Pt process deposition produces different values of SSE voltage signal for same thickness of the ferromagnet. Nonetheless, we will later show that the scaling of the SSE with the FM thickness for every series is independent of the Pt crystal quality. The measured voltage has been observed to increase when FM/NM interface is sharper for similar NM and FM thicknesses consistently with previous studies.[22]

To estimate both ANE and SSE coefficients we measured the transversal voltage as a function of the applied magnetic field at 300 and 70 K. That temperature selection was done taking into account that magnetite presents a metal to insulator transition at around 125 K called the Verwey transition. For this purpose, different gradients have been applied observing in all the cases a linear relation between the measured saturation voltage and the applied temperature gradient. The extracted voltage as a function of the applied magnetic field is similar to the one found in previous works.[4] The Spin Seebeck coefficient (SSC) is defined as the slope of the antisymmetric part to the signal $V_y^{antisym}$ ($V_y^{antisym} = [V_y(H_{sat}) - V_y(-H_{sat})]/2$, with $\mu_0 H_{sat} = 0.8$ T) vs the applied thermal gradient in the z direction (ΔT) after subtracting the ANE contribution and normalized with the sample geometry ($SSC = \frac{V_y^{antisym}}{\Delta T} \frac{L_Z}{L_Y}$). ANE was measured using the same configuration and experimental setup in Fe$_3$O$_4$ films. Samples with dimensions L$_X$=2 mm, L$_Y$=7 mm, and L$_Z$=0.5 mm are subjected to a thermal gradient in the vertical (z) direction. When a magnetic field is applied in plane, a transversal voltage is measured in the perpendicular direction.[4]

The major drawback concerning the longitudinal configuration for SSE measurements resides in the ANE contribution from the FM material to the observed voltage, especially for thick samples. To avoid this artifact, we need to carefully quantify the ANE voltage. This can be estimated as[4]

$$E^y = \left(\frac{r}{1+r}\right) E_{ANE}, \quad (1)$$

where E^y stands for the final contribution to the measured signal, E_{ANE} corresponds to the ANE voltage for every thickness measured in another piece of the same film without Pt and $r = \frac{\rho_{Pt}}{\rho_{Fe_3O_4}} \frac{t_{Fe_3O_4}}{t_{Pt}}$, with ρ representing the Pt and Fe$_3$O$_4$
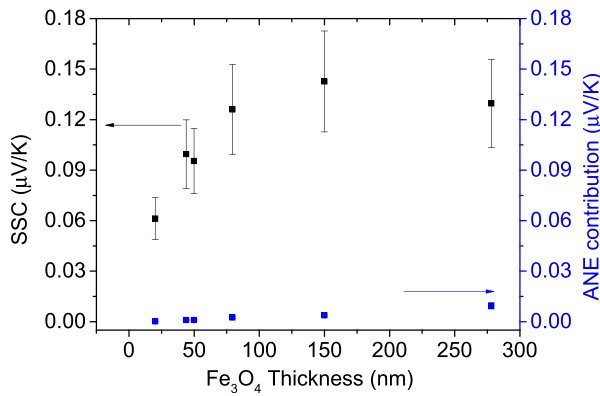
FIG. 2. ANE contribution to SSE as a function of magnetite thickness for the 14 nm RT Pt series at 300 K. SSC for the same series. Error bars represent the addition of both the uncertainty of the measurement and the average of a number of experiments in a control sample.

resistivity and t its thickness, respectively. Considering the series with 14 nm of Pt, in the worst case, for the thicker sample (280 nm), we obtain that the ANE contribution is about 7% of the obtained SSE signal at 300 K. For the 20 nm sample we obtain a contribution of 0.4%, clearly showing that the SSE dominates the measured voltage. ANE contribution calculated by Eq. (1) as a function of the film thickness for the sample series with 14 nm of Pt grown at RT, as well as the SSC for the same series, can be seen in Figure 2. Below the Verwey transition temperature magnetite is an insulator; therefore, ANE becomes negligible due to the reduction of the number of mobile charge carriers. Then, in the measurements of SSE at 70 K the ANE contribution is considered negligible. ANE contribution to SSE signal due to magnetic proximity must be additionally considered. Proximity ANE (PANE) measurements were performed in the perpendicular configuration[23] and the values are three orders of magnitude smaller compared with SSE measured in the LSSE configuration. In this configuration, the thermal gradient is applied in plane while the magnetic field is applied out of plane, so the SSE vanishes due to the direction of the injected spin current being parallel to the applied magnetic field.

For every series of Fe_3O_4/Pt bilayer the voltage increases with the film thickness and saturates at around 100 nm. Phenomenologically, the reason for this behavior can be found in the Gilbert damping constant (α). The largest changes in the magnetic damping occur for films of few monolayers thickness, while the values of α for ferromagnetic films tend to the corresponding bulk value with increasing film thickness.[24] Mathematically, the behavior can be described by the linear response theory.[15,16] According to this theory, two types of spin currents play the important role in the SSE: conduction electron spin current in the NM layer and magnon spin current in the FM layer. Adachi et al.[16] described the magnon current in the FM using the Landau–Lifshitz–Gilbert equation, introducing the spinwave approximation, and projecting the magnon current onto the spin quantization axis. Using the proper boundary conditions they calculated the magnon and spin accumulation and therefore the magnonic current in the FM. By analyzing this

dependence a characteristic length scale of the magnon accumulation (Λ) for magnetite can be estimated.

The proposed dependence by the Linear Response Theory for SSE[14,16–18] voltage is as follows:

$$V_{SSE} \propto \frac{(1 - 1/\cosh(L/\Lambda))(1 - 1/\cosh(l/\lambda))}{(\tanh(l/\lambda) + F_s)(\tanh(L/\Lambda) + F_m) - G_s G_m}, \quad (2)$$

where L, l, and λ stand for the FM thickness, NM thickness, and spin diffusion length in Pt, respectively, whereas G_s, G_m and F_m, F_s are constants dependent on the material.

Magnetite is an oxide material with semiconducting behavior, having a resistivity two orders of magnitude larger than that of Pt[4] and an increasing resistance upon temperature decrease. At temperatures below the Verwey transition, magnetite is an insulator. As much below as above the Verwey transition the linear response theory remains valid. The dependence of the Spin Seebeck Coefficient (SSC) at 300 K for the four different platinum deposition methods previously described is represented in Fig. 3; each series of measurements is normalized at the SSC of the 280 nm thickness. The dependence of the normalized SSC scales similarly for every series independently of the Pt deposition method. This allows to focus on the behavior of magnon current in the magnetic material without taking into account the Pt crystal quality.

We estimate a $\Lambda = 17 \pm 3$ nm at 300 K. The fit shown in Figure 3(a) corresponds to the 14 nm Pt grown at room
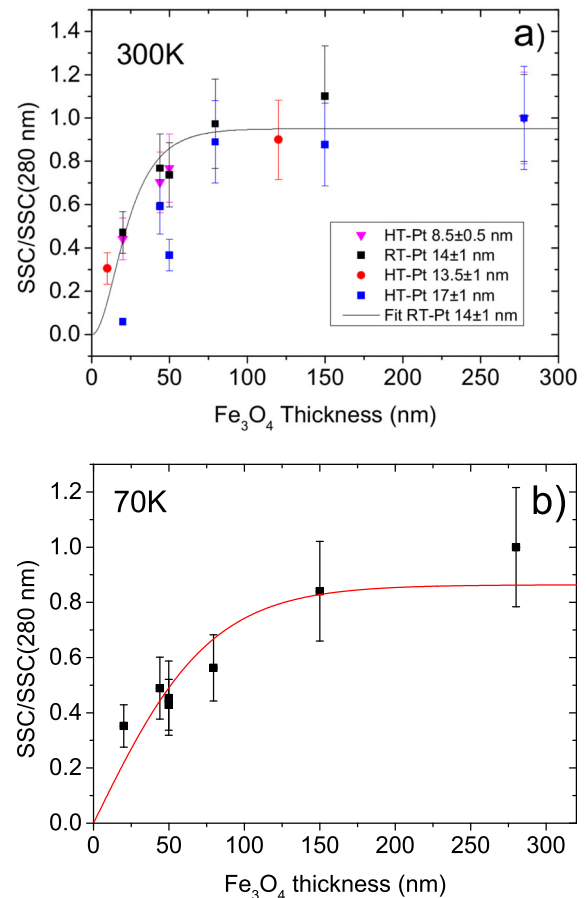

FIG. 3. (a)Dependence of the SSC normalized by the thickest sample in each series of Pt growth. (b) SSC for the series RT-Pt 14 ± 1 nm at 70 K and fit to the proposed dependence. The sample with 280 nm presents an SSC of 0.089 ± 0.001 μV/K.

temperature. Similar results have been found for the rest of the series. This result is one order of magnitude smaller than the reported values for other similar systems, such as YIG/Pt thin films.[6,25] The difference can be explained considering magnetite thin films' higher damping constant than YIG,[6,26] since Λ is considered to scale as the inverse of the damping constant.[27] Previous studies[11] have shown that SSE is suppressed at high magnetic fields, suggesting that low frequency magnons are important in SSE. This suppression is explained as an opening in magnon band gap due to Zeeman splitting, which does not affect high frequency magnons since their energy is much higher than the Zeeman energy. Therefore, high energy magnon contribution to SSE is expected to be weaker because they are closer to local thermal equilibrium due to their short thermalization lengths. At 70 K we have estimated $\Lambda = 40 \pm 10$ nm [Figure 3(b)]. The magnon–phonon interaction at lower temperatures is weaker due to the reduction of the number of phonons, allowing magnons to travel longer distances. This phenomenon is also observed in YIG.[6] This propagation length is highly dependent on system properties, such as the anisotropy or the damping parameter. It is important to notice that this value corresponds to the length scale of propagation for the magnons reaching the FM/NM interface only.[27]

In summary, we have studied the dependence of SSE with magnetite thin film thickness. The measured voltage presents a saturating behavior in agreement with reported models. From these models we are able to extract information about the length scale of the magnon accumulation. The SSE signal after subtracting the ANE contribution scales similarly for all the Pt series, ruling out any parasitic effect in the FM/NM interface or the Pt crystal quality. This represents the first measurement of Λ through Verwey transition. At lower temperatures, Λ increases due to the reduction in the number of phonons available for scattering with magnons.

[1]K. Uchida, S. Takahashi, K. Harii, J. Ieda, W. Koshibae, K. Ando, S. Maekawa, and E. Saitoh, Nature **455**, 778 (2008).
[2]K. Uchida, M. Ishida, T. Kikkawa, A. Kirihara, T. Murakami, and E. Saitoh, J. Phys.: Condens. Matter **26**, 343202 (2014).
[3]R. Ramos, M. H. Aguirre, A. Anadón, J. Blasco, I. Lucas, K. Uchida, P. A. Algarabel, L. Morellón, E. Saitoh, and M. R. Ibarra, Phys. Rev. B **90**, 054422 (2014).
[4]R. Ramos, T. Kikkawa, K. Uchida, H. Adachi, I. Lucas, M. H. Aguirre, P. Algarabel, L. Morellón, S. Maekawa, E. Saitoh, and M. R. Ibarra, Appl. Phys. Lett. **102**, 072413 (2013).
[5]S. M. Rezende, R. L. Rodríguez-Suárez, R. O. Cunha, A. R. Rodrigues, F. L. A. Machado, G. A. Fonseca Guerra, J. C. Lopez Ortiz, and A. Azevedo, Phys. Rev. B **89**, 014416 (2014).
[6]A. Kehlberger, U. Ritzmann, D. Hinzke, E.-J. Guo, J. Cramer, G. Jakob, M. C. Onbasli, D. H. Kim, C. A. Ross, M. B. Jungfleisch, B. Hillebrands, U. Nowak, and M. Kläui, Phys. Rev. Lett. **115**, 096602 (2015).
[7]J. Xiao, G. E. W. Bauer, K.-C. Uchida, E. Saitoh, and S. Maekawa, Phys. Rev. B **81**, 214418 (2010).
[8]E. Saitoh, M. Ueda, H. Miyajima, and G. Tatara, Appl. Phys. Lett. **88**, 182509 (2006).
[9]S. R. Boona and J. P. Heremans, Phys. Rev. B **90**, 064421 (2014).
[10]R. L. Douglass, Phys. Rev. **129**, 1132 (1963).
[11]T. Kikkawa, K.-I. Uchida, S. Daimon, Z. Qiu, Y. Shiomi, and E. Saitoh, Phys. Rev. B **92**, 064413 (2015).
[12]H. Jin, S. R. Boona, Z. Yang, R. C. Myers, and J. P. Heremans, Phys. Rev. B **92**, 054436 (2015).
[13]B. L. Giles, Z. Yang, J. S. Jamison, and R. C. Myers, Phys. Rev. B **92**, 224415 (2015).
[14]R. Ramos, T. Kikkawa, M. H. Aguirre, I. Lucas, A. Anadón, T. Oyake, K. Uchida, H. Adachi, J. Shiomi, P. A. Algarabel, L. Morellón, S. Maekawa, E. Saitoh, and M. R. Ibarra, Phys. Rev. B **92**, 220407(R) (2015).
[15]S. Hoffman, K. Sato, and Y. Tserkovnyak, Phys. Rev. B **88**, 064408 (2013).
[16]H. Adachi, K. Uchida, E. Saitoh, and S. Maekawa, Rep. Prog. Phys. **76**, 036501 (2013).
[17]S. S.-L. Zhang and S. Zhang, Phys. Rev. B **86**, 214424 (2012).
[18]S. Takahashi, E. Saitoh, and S. Maekawa, J. Phys.: Conf. Ser. **200**, 2030 (2010).
[19]J. De Teresa, A. Fernández-Pacheco, L. Morellon, J. Orna, J. Pardo, D. Serrate, P. Algarabel, and M. Ibarra, Microelectron. Eng. **84**, 1660 (2007).
[20]J. Orna, P. A. Algarabel, L. Morellón, J. A. Pardo, J. M. de Teresa, R. López Antón, F. Bartolomé, L. M. García, J. Bartolomé, J. C. Cezar, and A. Wildes, Phys. Rev. B **81**, 144420 (2010).
[21]M. Ziese and H. J. Blythe, J. Phys.: Condens. Matter **12**, 13 (2000).
[22]A. Aqeel, I. J. Vera-Marun, B. J. van Wees, and T. T. M. Palstra, J. Appl. Phys. **116**, 153705 (2014).
[23]K.-I. Uchida, T. Kikkawa, T. Seki, T. Oyake, J. Shiomi, Z. Qiu, K. Takanashi, and E. Saitoh, Phys. Rev. B **92**, 094414 (2015).
[24]E. Barati, M. Cinal, D. M. Edwards, and A. Umerski, Phys. Rev. B **90**, 014420 (2014).
[25]M. Agrawal, V. I. Vasyuchka, A. A. Serga, A. Kirihara, P. Pirro, T. Langner, M. B. Jungfleisch, A. V. Chumak, E. T. Papaioannou, and B. Hillebrands, Phys. Rev. B **89**, 1 (2014).
[26]S. Serrano-Guisan, H.-C. Wu, C. Boothman, M. Abid, B. S. Chun, I. V. Shvets, and H. W. Schumacher, J. Appl. Phys. **109**, 013907 (2011).
[27]U. Ritzmann, D. Hinzke, and U. Nowak, Phys. Rev. B **89**, 024409 (2014).